1

Developing elastic mechanisms: ultrafast motion and cavitation emerge at the millimeter

scale in juvenile snapping shrimp

Authors: Jacob S. Harrison¹ and S.N. Patek¹

¹ Department of Biology, Duke University, Durham, NC 27708, USA

Keywords: latch-mediated spring actuation, snapping shrimp, development, cavitation,

Alpheidae, elastic mechanism

Summary Statement:

Within 1-2 months after settlement, juvenile snapping shrimp develop an elastic mechanism

which allows them to generate ultrafast strikes, cavitation bubbles, and the highest recorded

accelerations for underwater, repeated-use movements.

Abstract:

1

2

3

4

5

6

7

8

9

10

11

12

13

14

15

16

17

18

19

20

Organisms such as jumping froghopper insects and punching mantis shrimp use springbased propulsion to achieve fast motion. Studies of elastic mechanisms primarily focus on fully developed and functional mechanisms in adult organisms. However, the ontogeny and development of these mechanisms can provide important insights into lower size limits of spring-based propulsion, the ecological or behavioral relevance of ultrafast movement, and the scaling of ultrafast movement. Here we examine the development of the spring-latch mechanism in the big claw snapping shrimp, Alpheus heterochaelis (Alpheidae). Adult snapping shrimp use an enlarged claw to produce high-speed strikes that generate cavitation bubbles. However, until now, it was unclear when the elastic mechanism emerges during development and whether juvenile snapping shrimp can generate cavitation at this size. We reared A. heterochaelis from eggs, through their larval and postlarval stages. Starting one month after hatching, the snapping shrimp snapping claw gradually developed a spring-actuated mechanism and began snapping. We used high speed videography (300,000 frames s⁻¹) to measure juvenile snaps. We discovered that juvenile snapping shrimp generate the highest recorded accelerations $(5.8 \times 10^5 \pm 3.3 \times 10^5 \text{ m s}^{-2})$ for repeated use, underwater motion and are capable of producing cavitation at the millimeter scale. The angular velocity of snaps did not change as juveniles grew; however, juvenile snapping shrimp with larger claws produced faster linear speeds and generated larger, longer-lasting cavitation bubbles. These findings establish the development of the elastic mechanism and cavitation in snapping shrimp and provide insights into early life-history transitions in spring-actuated mechanisms.

Introduction:

Biological systems achieve ultrafast motion through latch-mediated spring actuation (LaMSA), a process that uses intricately coordinated springs and latches to temporarily store and then rapidly release elastic energy to propel movement (Bennet-Clark, 1975; Gronenberg, 1996; Longo et al., 2019; Patek et al., 2004; Patek et al., 2011). LaMSA mechanisms have repeatedly evolved across the tree of life, leading to incredible behaviors such as legless larval flies leaping through the air (Farley et al., 2019), plants shooting ballistic seed projectiles (Hofhuis et al., 2016), and mantis shrimp generating high speed strikes to capture or process their prey (Patek, 2019; Patek et al., 2004). LaMSA research largely focuses on mechanisms within a narrow size or age range of the organism; however, the biomechanics of an organism changes over ontogeny as the underlying mechanical systems change in size and shape (Herrel and Gibb, 2006).

Identifying when LaMSA elements develop and how development coincides with the emergence of behavior can help elucidate how a biomechanical system relates to ecological shifts in early life history. Mantis shrimp develop their LaMSA mechanism as they transition to the pelagic zone and begin feeding (Harrison et al., 2021). During this transition, mantis shrimp develop the saddle and meral-v, both elastic elements found in the adult mantis shrimp LaMSA mechanism (Patek et al., 2007; Rosario and Patek, 2015; Zack et al., 2009). Biological LaMSA mechanisms are often complex mechanical systems that integrate multiple elements, including motors (e.g., muscles), springs (e.g., tendon, apodeme), and latches (Anderson et al., 2014; Blanco and Patek, 2014; Claverie and Patek, 2013; Longo et al., 2019); understanding when and how these mechanisms develop within systems helps inform the ecological and evolutionary relevance of spring actuation in biology (Roberts and Azizi, 2011; Wood, 2020).

Ontogeny and development are also useful in exploring scaling constraints on the size and kinematics of biomechanical systems (Dangles et al., 2007; Herrel and Gibb, 2006; Kolmann and Huber, 2009; Tanner et al., 2010; Vincent et al., 2007). For example, the negative scaling coefficients for feeding kinematics and morphology in first-feeding zebrafish larvae reflect the challenges of a viscous-dominated fluid environment (Hernandez, 2000). During early life history stages, the larval operculum is underdeveloped, and the relative water viscosity is much greater. At these small sizes, larval feeding is likely constrained by the time it takes to force

viscous water out of the buccal chamber (Hernandez, 2000). Mathematical and physical models of LaMSA mechanisms suggest that smaller LaMSA mechanisms deliver elastic energy more efficiently and generate greater accelerations than larger LaMSA mechanisms (Ilton et al., 2018; Ilton et al., 2019). Comparative studies of the scaling of LaMSA kinematics provide mixed support for these models (Ilton et al., 2018; Sutton et al., 2019). The phylogenetic variation inherent in broad comparative datasets can make it difficult to disentangle variables and isolate the effects of size (Freckleton and Jetz, 2009; Muñoz, 2022). For example, even though a jellyfish nematocyst and a locust jumping leg both use elastic recoil to achieve ultrafast movement, they use different physical structures for different behaviors. Ontogenetic scaling of LaMSA morphology and performance can provide important insights into how growth and size affect function within a system and whether that agrees with mathematical models or larger comparative studies.

Here we establish the development and scaling of LaMSA in snapping shrimp. Snapping shrimp (Alpheidae) are a clade of decapod crustaceans that use a LaMSA mechanism in their enlarged, specialized claw to generate cavitation bubbles (Fig 1; Anker et al., 2006; Dinh and Patek; Kaji et al., 2018; Kingston et al., 2022). Cavitation is an incredibly energetic event that occurs when liquid water briefly vaporizes and implodes; the collapse of the bubble releases energy in the form of light, heat, and sound (Brennan, 1995). Adult snapping shrimp create these bubbles by rapidly inserting a plunger on their dactyl into a corresponding socket on their propodus, and thereby ejecting a high-speed jet of water and cavitation bubble (Versluis et al., 2000). Substantial prior research addresses snapping shrimp behavior (e.g., Dinh et al., 2020; Hughes, 1996; Nolan and Salmon, 1970; Schein, 1977), evolution (e.g. - (e.g., Anker et al., 2006; Chow et al., 2021; Kaji et al., 2018), development (e.g., Knowlton, 1973; Spence and Knowlton, 2008), biomechanics (e.g., Kim et al., 2010; Lohse et al., 2001; Ritzmann, 1974; Versluis et al., 2000; Yang et al., 2020), and ecology (e.g., Butler et al., 2017; Mathews et al., 2002). A previous study on snapping shrimp development showed that the postlarval claws were undifferentiated (Young et al., 1994), which suggests that snapping shrimp do not have a LaMSA mechanism when they settle in adult habitats. Even so, to our knowledge, research has not addressed the

timing and emergence of the snapping behavior during development, the scaling of snap kinematics, and the threshold size and kinematics that successfully produce cavitation.

Here we address three central questions. (1) At what size and age do snapping shrimp develop their LaMSA mechanism? (2) Is the LaMSA mechanism capable of generating cavitation at this size? (3) How do claw kinematics compare to adult snapping shrimp and other biological LaMSA mechanisms? To address these questions, we reared snapping shrimp larvae through early development and established when the snapping claw, snapping behavior, and cavitation bubbles emerged. We then compared juvenile snapping shrimp strike kinematics with adult kinematics and with other high-acceleration biological systems collected from the literature. Based on comparative studies and mathematical models, we predicted that snapping shrimp would develop their LaMSA mechanism shortly after the larvae transition into the adult habitats and that juvenile snapping shrimp would generate accelerations greater than their adult counterparts (Ilton et al., 2018).

Methods:

Specimen collection and claw development:

As our egg source for the ontogenetic study, we collected four gravid female *Alpheus heterochaelis* from mudflats in Beaufort, NC in July 2020. Female snapping shrimp adhere their developing eggs to their pleopods. We carefully scraped the eggs off the pleopods and placed them into 10x10x10 cm³ plastic containers filled with synthetic seawater. Synthetic seawater was made by mixing sea salt (Instant Ocean, Spectrum Brands, Blacksburg, VA,USA) into RO grade fresh water (temp: ~27 °C, salinity: ~30 ppt). Containers were gently rocked on a variable speed shaker table, which kept water continually flowing over the eggs. Within 20 days, hatching ended. Newly hatched larvae were kept under the same conditions as the eggs and inspected daily to determine the timing of larval molts. After 5-6 days, all larvae completed their three pelagic larval stages and settled as postlarva (Fig 1; Knowlton, 1973). Postlarvae were taken off the shaker table and transferred into individual plastic containers filled with synthetic seawater and kept under ambient light. At the postlarval stage, snapping shrimp began feeding on one- to two-day-old *Artemia* nauplii (Grade A Brine Shrimp Eggs, Brine Shrimp Direct, Ogden, UT, USA). Snapping shrimp were fed daily. Their containers were cleaned every 1-2 days. Cleaning consisted of a 50% water change and removal of old food and detritus.

Around one-month post settlement, juvenile snapping shrimp began snapping their major chelae during water changes and feedings. Over three weeks, we selected 20 juvenile shrimp from each of the four egg clutches (5 individuals per clutch) to visualize and measure striking behavior. Individuals were chosen to encompass a range of body sizes present in each egg clutch at the time of data collection (SFig. 1).

Strike and Cavitation Probability:

Juvenile snapping shrimp strikes (281 strikes, 20 individuals, 3-15 strikes per individual) were collected using a high speed video camera attached to a microscope (model 165M FC stereomicroscope, Leica Microsystems Inc., Buffalo Grove, IL, USA; 256x128 pixel resolution, 300,000 frames s⁻¹, Fastcam SA-Z, Photron, San Diego, CA, USA). To film juvenile strikes, we removed each individual from its container, dried the carapace with a paper towel, and affixed a toothpick to the carapace using cyanoacrylate glue. We held the toothpick and snapping shrimp in place using small clamps. We then filmed the strikes using a dorsal view and attempted to elicit fifteen strikes from each individual by agitating them with a toothpick. A maximum of fifteen strikes for each snapping shrimp was decided prior to data collection. Out of the twenty individuals tested, only two stopped striking before reaching fifteen strikes (one individual struck only 3 times and another individual struck only 8 times). Because we were unable to track individual molts for all snapping shrimp across our experiment, measurements of snapping shrimp reflect size and not a specific molt. High speed video was collected for each strike attempt. We defined a strike attempt as follows: an individual cocks the dactyl open, directs the claw away from the body, and rapidly rotates the dactyl. Videos were calibrated using a 0.1 mm-scale ruler (PEAK 1972-50 Glass scale; GWJ Company, La Quinta, CA, USA) filmed in the plane of focus.

Strike attempts were binned into two categories: full strikes and incomplete strikes. If the dactyl completely closed against the propodus during a strike attempt, it was considered a full strike (Movie 1). If the dactyl did not fully close, we considered it an incomplete strike (Movie 2). Full strikes were further categorized by whether they generated a cavitation bubble or not. If a strike generated a cavitation bubble, we measured the distance each bubble traveled and the duration of bubble collapse. Bubble travel distance was defined as the linear distance between the location of collapse from the edge of the propodus socket. Collapse

duration was defined as the length of time between the bubble's maximum size and when the bubble collapsed. Statistical tests comparing snapping shrimp size and strike probabilities are outlined below.

Strike Kinematics:

Of the 281 strikes collected from juvenile snapping shrimp, only 125 (19 individuals, 2 - 13 per individual) were full strikes and in the proper orientation for kinematic analyses. We manually tracked four points on the snapping claw: two points on the dactyl and two points on the propodus (DLTdv7 MATLAB script; MATLAB 9.4, version R2018a; Hedrick, 2008). Point tracking began one frame before dactyl rotation and ended when the dactyl fully closed. Tracked points were converted into angular displacement and smoothed using a LOESS model fit. Angular velocity was calculated from the first derivative of the fitted positional data with respect to time. Angular acceleration was calculated from the first derivative of a LOESS model fit to the angular velocity (Fig. 3). One random strike was digitized 10 times to calculate the digitizing error. The standard error of the reported mean from digitizing constituted 0.7% of the reported rotation measurement, 0.8% of the velocity measurement, and 1.4% of the acceleration measurement.

After filming, we fixed individuals in 4% glutaraldehyde with 0.2 M PBS and 8% sucrose mixture. After fixation, we imaged each snapping shrimp, surgically removed their snapping claws, and then imaged the dorsal, lateral, and ventral facing sides of each claw (2560x1920 pixel resolution; DFC 450 C camera; model 165M FC microscope; Leica Microsystems Inc., Buffalo Grove, IL, USA). Each image was embedded with a digital scale bar calibrated using a 0.02 mm stage micrometer. Claws were weighed using a microbalance (resolution: 1 µg; XPE56 Mettler Toledo, Pleasant Prairie, WI, USA). Finally, the dactyl was surgically removed from the propodus and weighed. During one of the dissections, one dactyl was accidentally lost, therefore, we only report dactyl mass for 19 individuals (Table S1).

We measured the carapace length, snapping claw length, dactyl length, and plunger distance from microscope images of each snapping shrimp (Image J, V2.1.0; National Institute of Health, Bethesda, MD, USA; Schneider et al., 2012). Carapace length was defined as the distance from the tip of the rostrum to the posterior edge of the carapace at the midline. Snapping claw length was defined as the distance from the joint between the propodus and

carpus to the distal-most point on the dactyl. Dactyl length was defined as the distance from the point of rotation on the propodus to the dactyl tip. Plunger distance was defined as the distance between the point of rotation and the apex of the plunger. Morphological measurements are illustrated in Figure S#. To reduce the effect of measurement error, all mass and length measurements were collected three times each and we report the mean value here. Plunger speed was calculated by multiplying the angular velocity in radians per second by the plunger distance. Linear acceleration of the claw was calculated by multiplying the angular acceleration in radians per second squared by dactyl length. Statistical tests comparing strike kinematics and snapping shrimp size are further outlined below. It is important to note that we cannot differentiate between size and age within juvenile snapping shrimp.

Evidence of LaMSA in juvenile snapping shrimp:

Using the kinematics and morphology measured above, we estimated the power density required to rotate the snapping shrimp dactyl during a strike. We used a similar approach developed for measuring mantis shrimp energetics (McHenry et al., 2012). During a snapping shrimp strike, both the dactyl and propodus rotate through the water. Given the complexities of modeling multiple rotations at high rates in tiny structures, we simplified the model to only include the rotation of the dactyl. This is a conservative approach to measuring power density because it underestimates total strike energy by not including propodus rotation. We approximated total strike energy (E_{strike}) as:

$$E_{strike} = E_{KE} + E_d$$

Where E_{KE} is the kinetic energy of the strike and E_d is the energetic cost of drag.

Strike kinetic energy (E_{KE}) generated during claw closure was calculated as:

$$E_{KE} = \frac{I_{Dactyl} + I_{Water}}{2} \omega^2,$$

where I is the moment of inertia and ω is the angular velocity of the strike. The moment of inertia of the dactyl was calculated using a blade element approach (McHenry et al., 2012; McHenry et al., 2016). Using microscope images of snapping shrimp claws, we divided the dactyl into twenty different chord-wise elements along its length (Fig. S2). For each element, we measured the chord thickness (i.e., linear dimension along the length of the dactyl), chord length (i.e., linear dimension parallel to the flow), chord width (i.e., linear dimension

perpendicular to the flow), and the distance from the center of each element to the point of rotation. The volume of each element was approximated using the calculation for an elliptical cylinder. We assigned a mass for each element by taking the mass of the entire dactyl and then assigning a mass proportional to the element's relative volume. We then calculated the moment of inertia for the dactyl by summing the moment of inertia for each individual element:

204
$$I_{Dactyl} = \sum_{i=1}^{n} m_i + r_i^2$$
,

198

199

200

201

202

203

207

208

215

216

where m_i is the mass of each element, r_i is the distance of each element from the point of rotation.

The dactyl accelerates an added mass of water which is proportional to the moment of inertia of the water, *I*_{water} was calculated using the following equation (Sarpkaya, 1986):

$$I_{water} = \frac{1}{4} \pi \rho_{water} \int_0^L r^2 h^2 dL,$$

- Where *h* is the chord width, *r* is the distance from the point of rotation, and *L* is the length of the dactyl.
- The energetic cost of drag (E_d) was calculated by integrating the drag torque (τ_{drag}) over the angular displacement of the strike (McHenry et al., 2012):

$$E_d = \int_0^{\gamma_d} \tau_{drag} d\gamma,$$

- where γ_d is the total angular excursion of the strike. This integral was solved using the cumtrapz function in R (cumtrapz, R v.1.3.959).
- We modeled torque created by drag on the dactyl with the same blade-element approach which integrates the force generated by elements along the length of the dactyl.
- Torque was calculated with the following equation (Hoerner, 1965):

$$\tau_{drag} = \frac{1}{2} \rho T_d L^5 \left(\frac{d\gamma}{dt}\right)^2,$$

where $\frac{d\gamma}{dt}$ is the angular velocity, L is the length of the dactyl, ρ is the density of water (1025 kg m⁻³) and T_d is the drag-torque index. The drag-torque index is a dimensionless number calculated by approximating the shape of the rotating structure as an elliptical cylinder (McHenry et al., 2012). The number indicates the degree to which the rotating structure

generates drag as it rotates through a fluid. We calculated T_d using the equation (McHenry et al., 2012):

227
$$T_{d} = \frac{1}{L^{5}} \sum_{i=1}^{n} h_{i}(C_{d})_{i} r_{i}^{3} \Delta l,$$

where Δl is the thickness of each element, r is the distance between each element and the point of rotation, C_d is the drag coefficient of the element, and h is the width of the element. The drag coefficient (C_d) was calculated for each individual element by modeling a uniform elliptical cylinder (Hoerner, 1965):

$$C_d = k \left(1 + \frac{c}{h} \right) + 1.1 \left(\frac{h}{c} \right),$$

where c is the chord length and k is a shape coefficient that varies with the geometry of the structure. For a uniform elliptical cylinder, a fixed value (k=0.015) is predictive of empirical drag measurements (Hoerner, 1965). Morphological measurements taken for energy calculations are shown in Figure S2.

Finally, we divided the total strike energy by strike duration and snapping claw mass to determine the mass-specific maximum power output of the strike. We compared the modeled power outputs of the juvenile snapping shrimp strikes to the previously measured maximum power outputs of muscle (1200 W kg⁻¹ in *Coturnix chinensis*; Askew et al., 2001).

We performed error (uncertainty) analyses for strike kinematics and energy calculations based on the uncertainty of the mass (5 x 10^{-10} kg), distance (5 x 10^{-5} m), and time measurements (300,000 frames s⁻¹; 1.5 x 10^{-7} s). The resulting uncertainty in our reported calculations ranged from 10.3 to 20.3% (speed: 10.3%, acceleration:10.4%; Energy: 10.3%; Power Density: 20.3%) and is represented via the significant digits reported in Table 1.

LaMSA mechanism:

Adult *A. heterochaelis* use a torque-reversal latch to mediate the flow of elastic energy in their snapping claw (Ritzmann, 1974; Longo et al., *in revision*). In adults, unlatching is achieved via a "trigger muscle", a section of the closer muscle that originates along the anterior medial edge of the propodus (Ritzmann, 1974; Kaji et al., 2018). We looked for the development of the trigger muscle in juvenile *A. heterochaelis* to determine whether juveniles use a similar torque-reversal latch for their LaMSA mechanism. The propodus is slightly transparent in juvenile snapping shrimp, so we used images taken of snapping claws under the

microscope to determine the presence or absence of the trigger muscle. We used microscope images of developing *A. heterochaelis* snapping claws to look for the development of the saddle-like regions in juvenile snapping shrimp (Fig. 1).

Kinematic Comparisons:

Finally, we compared juvenile snapping shrimp strike accelerations to adult *A. heterochaelis* strikes and other biological LaMSA mechanisms. Adult *A. heterochaelis* strike accelerations were calculated by Versluis et al., 2000; however, they did not report the mass of the snapping claw or dactyl. We weighed snapping claws and dactyls from adult *A. heterochaelis* collected in Beaufort, North Carolina (n=3). We then used the dactyl mass from juvenile and adult snapping claws for our kinematic comparisons. Our larger comparative dataset was expanded from a previously-compiled dataset of LaMSA mechanisms (Ilton et al., 2018; Longo et al., 2021). We added a series of recently reported high-acceleration systems including larval mantis shrimp (Harrison et al., 2021), larval dragonfly (Büsse et al., 2021), trapjaw spider (Wood, 2020), slingshot spiders (Alexander and Bhamla, 2020), larval bark beetles (Bertone et al., 2022), thirteen species of trap-jaw ants (Booher et al., 2021; Gibson et al., 2018; Larabee et al., 2017), and seventy-seven species of frogs (Mendoza et al., 2020; Moen et al., 2013; Moen et al., 2021).

Statistical Analyses:

We used one-way ANOVAs to test whether body mass or snapping claw mass differed between egg clutches. We then used a major axis regression between log-transformed claw mass and log-transformed body mass to determine whether snapping claw growth was positively allometric across individuals (ma function; smatr; Warton et al., 2012). The slope of the major axis regression was evaluated against a null hypothesis of isometry (slope of 1).

To determine whether larger claws were more likely to produce full strikes than smaller claws we binned individuals into two groups: (1) individuals that produced full strikes 100% of the time and (2) individuals that sometimes produced incomplete strikes. We ran a Welch Two Sample t-test comparing snapping claw mass between the two groups (20 individuals; Fig 4A). We then repeated this test using cavitation probability to determine whether larger claws were more reliable at producing cavitation bubbles. This t-test only included data from full strikes (n=19 individuals; Fig 4B).

Finally, we tested how bubble travel distance, bubble collapse duration, maximum angular velocity, and maximum plunger speed scaled with claw mass using linear models (Im function; Imer package, R v.1.3.959). Linear models for bubble travel distance and collapse duration only included strikes that produced cavitation bubbles (216 strikes, 16 individuals, 4 to 15 strikes per individual). Linear models for maximum angular velocity and plunger speed only included strikes for which we measured strike kinematics (125 strikes, 19 individuals, 2 to 13 strikes per individual).

Results:

284

285

286

287

288

289

290

291

292

293

294

295

296

297

298

299

300

301

302

303

304

305

306

307

308

309

310

311

312

Snapping Shrimp Development

We successfully hatched and raised A. heterochaelis eggs through their pelagic larval phase into the postlarval and juvenile stages. The entire larval pelagic phase of A. heterochaelis was complete after roughly five days. This phase consisted of three pelagic larval stages separated by discrete molting cycles. During the first and second larval stages, larvae had three pairs of swimming appendages, while in the third and final larval stage larvae had six pairs of swimming appendages (Fig 1). After settlement, the six sets of swimming appendages transformed into six sets of pereopods: three anterior sets of chelae and three posterior sets of walking appendages (Fig 1). The first pereopods started as undifferentiated chelae and over a two-month period, they gradually differentiated into the major and minor chelae (snapping and non-snapping claws). After the third or fourth molt, the snapping claw began forming a plunger and socket. At this same time, the propodus developed two saddle-like shapes on the lateral and medial sides of the claw (Fig. 1). Over several molts, the plunger and socket deepened, and two saddle-like shapes become more pronounced. At the same time, the closer muscle inside the propodus developed new origin sites along the propodus that correspond with the trigger muscle seen in adult A. heterochaelis (Ritzmann, 1974). Roughly one month after settlement (~5-6 molts), juvenile A. heterochaelis began snapping during feedings and water changes (J. Harrison pers. obsv.). After two months (~8-9 molts), juvenile snapping claws showed remarkable similarity to adult snapping claws.

We found no statistical difference in body mass or snapping claw mass between clutches (body mass: df= 3, F= 0.0722, p= 0.974; snapping claw mass: df=3, F= 0.1819,

p=0.9071). However, juvenile snapping claw mass was positively allometric relative to carapace length during this early period of growth (Fig. 2; slope = 1.7, R^2 = 0.91, p<0.001, df = 18).

Strike and Cavitation Probability

Starting one-month post-settlement, juvenile snapping shrimp began striking. During a strike, juvenile snapping shrimp extended their major claw away from the body, fully opened their propodus (~90-100 degrees), held the dactyl open for roughly 500 ms, and then rapidly closed the dactyl. We attempted to elicit fifteen strikes from twenty juvenile snapping shrimp; however, two individuals stopped striking before we reached 15 strike attempts. Our final dataset was comprised of 281 strike attempts across twenty individuals (3-15 strikes per individual). We were unable to elicit strikes from juvenile snapping shrimp smaller than 3 mm in carapace length. Snapping shrimp with larger claws were more reliable at producing full strikes (Fig 4A; t=-3.6887, df=9.9652, p= 0.00421) and more reliable at producing cavitation bubbles (Fig 4B; t=-3.441, df=16.054, p = 0.00334). This means that larger snapping shrimp were more likely than smaller snapping shrimp to produce full strikes and those strikes were more likely to generate cavitation bubbles. Only 24 out of 240 full strikes did not produce cavitation bubbles. Juvenile snapping shrimp with claws larger than 2 x 10-6 kg produced full, cavitating strikes every time we attempted to elicit a strike (Fig 4).

Strike Kinematics and LaMSA

Maximum angular velocity did not vary with the size of the snapping claw (Fig 5A; n=125 strikes, 19 individuals, 2-13 strikes per individual). However, snapping shrimp with larger claws produced greater linear speeds (Fig 5B; R^2 =0.175, F-statistic=4.821, p<0.05, df=17). Maximum linear acceleration of the juvenile snapping shrimp strike was on average 5.464 x $10^5 \pm 1.621$ x 10^5 m s⁻², two orders of magnitude greater than adult *A. heterochaelis* strikes (7.2 x 10^3 m s⁻²; Versluis et al., 2000). Notably, peak acceleration of juvenile strikes generally occurred well after the dactyl started rotating (Fig 3D). Juvenile snapping shrimp with larger claws produced longer-lasting bubbles that traveled further (Fig 5C,D; bubble duration: R^2 =0.843, F-statistic = 81.42, p<0.001, df= 14; bubble distance: : R^2 =0.90, F-statistic = 133.377, p<0.001, df= 14). Average strike kinematics are reported in Table 1.

Mass-specific power of juvenile snapping shrimp strikes was on average $4.33 \times 10^7 \pm 2.185 \times 10^7 \, \text{W kg}^{-1}$ (Fig 6). These measurements far exceed the maximum measured power

output recorded for vertebrate muscle (1200 W kg⁻¹; Askew et al., 2001). The power density of juvenile snapping shrimp strikes is similar to Dracula ants ($5.0x10^6$ W kg⁻¹; Larabee et al., 2018) and snapping termites ($1.1x10^7$ W/kg; Seid et al., 2008).

Discussion:

Juvenile *A. heterochaelis* use a LaMSA mechanism that generates the highest recorded accelerations measured for underwater, repeated-use, ultrafast movements (Fig 7). Our study shows that the LaMSA morphology and snapping behavior develop gradually between one- and two-months post-settlement (Fig 1). The spring-actuated strikes of these juvenile snapping shrimp are so fast that they form cavitation bubbles, even in claws smaller than 1 mg (Fig 4). Larger juvenile snapping shrimp have larger snapping claws, which are more likely to produce full, cavitating strikes than smaller snapping claws (Fig 4A,B). Angular velocity does not change with claw size (Fig 5A); however, larger claws produced faster linear speeds and longer-lasting bubbles (Fig 5B-D). The average power density for juvenile strikes (4.3 x $10^7 \pm 3.7 \times 10^7 \text{ W kg}^{-1}$) exceeds known muscle power limits and strongly suggests a LaMSA mechanism (Fig 6). Joint morphology and muscle orientation suggest that juvenile *A. heterochaeilis* use a similar torquereversal latch found in adults. We explore these results in the context of snapping shrimp development and ecology, other biological LaMSA mechanisms, and the implications of biological limits for spring-actuated movements.

Timing of claw development and striking behavior:

Snapping claw development in *A. heterochaelis* is a gradual process that begins several weeks after larvae have settled. *Alpheus heterochaelis* undergo an abbreviated pelagic larval phase when individuals hatch as advanced zoeae, molt twice, and eventually settle out as postlarvae in adult habitats (Fig 1; Knowlton, 1973). Larval stages take roughly five days, during which the larvae do not feed and exhibit almost no growth (Knowlton, 1973). We initially predicted that snapping shrimp would develop their LaMSA morphology during the postlarval transition when they first enter adult habitats. However, an earlier study showed that postlarval *A. heterochaelis* reared in the lab did not possess snapping claws (Young et al., 1994). Here we support Young et al.'s findings, and further show that the timing of LaMSA morphogenesis occurs between one- and two months after settlement (Fig 1). This gradual differentiation of the snapping claw over several molts in juvenile snapping shrimp is

remarkably similar to snapping claw regeneration in adult *A. heterochaelis* (Govind et al., 1988). We see several distinct morphological shifts in the developing claw (Fig 1). For example, the plunger and socket gradually increase in relative size as the snapping shrimp grow. Likewise, the two saddle-like regions on the propodus become more apparent in the larger juveniles. A deeper understanding of the genetic drivers of claw development and how they relate to tissue differentiation and growth within the claw will further elucidate why the transition to striking behavior occurs at this age and size in snapping shrimp.

Development of the snapping claw corresponded with the onset of striking behavior in juvenile snapping shrimp, although not all strike attempts were successful. Smaller snapping shrimp, without fully developed snapping claws, were less likely to produce full, cavitating strikes compared to the larger and older juveniles (Fig 4A,B). Of the individuals we tested, the snapping shrimp with the smallest claw mass was unable to achieve complete claw closure during any of its fifteen strike attempts. We were also unable to elicit strikes from any snapping shrimp with claw mass less than 0.03 mg, likely because the spring-latch mechanism was not fully developed at that size. It is also noteworthy that both of the snapping shrimp that stopped striking before we reached our maximum fifteen strikes were among the smallest we tested.

Even at millimeter size scales, juvenile snapping shrimp move rapidly enough to generate cavitation. Cavitation is a highly energetic event: the collapse of the bubble generates light, heat, plasma, and the distinct popping sound that gives the animals their name (Kim et al., 2010; Lohse et al., 2001; Tang and Staack, 2019). The cavitation bubble in adult snapping shrimp is formed by a vortex of water ejected from the snapping claw when the plunger is rapidly rotated into the corresponding socket on the propodus (Hess et al., 2013). In juvenile snapping shrimp, claw size is crucial in the formation and ejection of these bubbles (Fig 4B). Snapping shrimp with snapping claws smaller than 1 mg did not always cavitate, even if they achieved a full strike (Fig 4B). Interestingly, smaller juvenile snapping shrimp were able to rotate their dactyls just as quickly as larger juveniles (Fig 5A), although larger snapping shrimp with longer dactyls could generate slightly higher speeds (Fig 5B). However, even though they are not moving much faster, snapping shrimp with larger claws generated cavitation bubbles that lasted significantly longer and traveled further than snapping shrimp with smaller claws

(Fig 5C,D). This is likely because the larger juveniles have more a pronounced plunger on the dactyl (Fig 1), which would eject a greater volume of water. The formation of the cavitation bubble is likely only possible when the snapping claw can generate a vortex of water with sufficient volume and speed. Further research into the fluid dynamics of the water jet during claw development will help elucidate how this vortex is formed and what is necessary to generate a cavitation bubble.

402

403

404

405

406

407

408

409

410

411

412

413

414

415

416

417

418

419

420

421

422

423

424

425

426

427

428

429

These results lead to several questions. Why do smaller claws strike and cavitate less reliably? At smaller sizes, it may be more difficult for A. heterochaelis to engage and maintain the geometric latching mechanism. At smaller sizes, smaller movements are necessary to unlatch the mechanism, increasing the potential risk to trigger the mechanism before it was fully loaded. Additionally, smaller claws may not have the right tuning between spring stiffness and muscle power. If the muscle cannot load the spring effectively, the mechanism will not be able to store the elastic energy necessary to rotate the dactyl at sufficient speeds. However, it is also important to mention that even though we labeled some strikes as unsuccessful, these movements were still ultrafast (<1 ms). Why would snapping shrimp attempt to strike if the mechanism is not reliable? Snapping shrimp use their snapping claws in antagonistic interactions with conspecifics or predators (Nolan and Salmon, 1970). Adult snapping shrimp use open snapping claws as a visual indicator of the size and competitive ability of their opponents (Hughes, 1996). Even if juvenile claws are not snapping reliably, the juvenile may still be signaling with the claw when it opens and it may be directing the claw towards an opponent or aggressor. Alternatively, juveniles may be "practicing" their strikes. Mechanical forces play an important role in the normal development and growth of musculoskeletal systems (Nowlan et al., 2010). For example, jaw opening behaviors during early development in larval zebrafish mechanically control joint morphogenesis and chondrocyte maturation through the Wnt signaling pathway (Brunt et al., 2017). The formation of myotendinous junctions in Drosophila indirect flight muscles requires mechanical signaling from tendon cells during embryogenesis (Fernandes et al., 1996). Loading and firing their LaMSA mechanism during early ontogeny may help juvenile snapping shrimp develop their snapping claw.

Even at the millimeter size, juvenile snapping shrimp are capable of projecting cavitation bubbles that travel almost twice the length of their dactyls (Fig 5C). We initially predicted that juvenile snapping shrimp would develop their snapping claw when they transitioned into adult habitats after settlement. Instead, we found that the development of the snapping claw is delayed nearly a month after settlement. However, shortly after the claw is developed, snapping shrimp are capable of projecting cavitation bubbles several millimeters. Snapping shrimp use cavitation bubbles in agonistic encounters with conspecifics and predators (Nolan and Salmon, 1970). Projection of the bubble beyond the length of their claw is a critical step for juvenile snapping shrimp to begin engaging in contests over resources and defending themselves against predators.

Evidence of LaMSA in juvenile snapping shrimp:

Evidence for the juvenile snapping shrimp LaMSA mechanism comes from their ultrafast kinematics and our approximations of the power required to produce the strike. Claw closure duration of juvenile snapping shrimp strikes ranged from 0.2 to 0.6 ms (Table 1). Larger juvenile snapping shrimp exhibited the longest durations. Peak angular velocities of juvenile strikes exceeded 22,000 radians per second (>1,200,000 ° s⁻¹). This is of a similar order of magnitude as the LaMSA strike in the Dracula ants (*Mystrium camillae*, 56,000 rad s⁻¹; Larabee et al., 2018). In comparison, King prawns (*Litopenaeus vannamei*) are a group of shrimp that do not use spring actuation to close the claws: their angular velocity clocks in at only 56.5 radians per second (Kaji et al., 2018).

The peak power density for juvenile snapping shrimp strikes was approximated as 4.27 x 10^7 W kg⁻¹. Similar orders-of-magnitude are present in the Dracula ant (5 x 10^6 W kg⁻¹; Larabee et al., 2018) and termite soldier strikes (1.1 x 10^7 W kg⁻¹; Seid et al., 2008). Every juvenile snapping shrimp strike showed power densities several orders of magnitude higher than the maximum measured power density of muscle (1121 W/kg in *Coturnix chinensis*; Askew et al., 2001). Therefore, the juvenile snapping shrimp strike must use spring actuation. Determining whether or not LaMSA is present through calculations of power density is particularly useful when direct measurements of spring dynamics are not feasible (Larabee et al., 2018; Longo et al., 2019; Patek et al., 2004). As discussed in the Methods section, the blade element models we used to approximate power density likely underestimate the amount of fluid drag.

Therefore, our calculations of energy and power underestimate the actual power requirements needed for snapping shrimp strikes.

Juvenile A. heterochaelis likely use the same torque-reversal latching mechanism as adults (Kaji et al., 2018; Ritzmann, 1974). Torque-reversal latches restrict the flow of energy when the mechanism is in a particular geometric configuration (Longo et al., 2019). When the snapping shrimp claw is open, a large portion of the closing muscle places a torque on the dactyl that keeps the dactyl open. When the latch is engaged, the muscles load elastic energy into elastic elements in the claw (Longo et al., In review). Unlatching occurs when a trigger muscle (a section of the closer muscle) shifts the direction of loading around the pivot point, thereby reversing the torque sign and rapidly closing the claw (Longo et al., In review; Ritzmann, 1974). A juvenile snapping shrimp claw that can generate high-speed strikes has a closer muscle along the medial facing side of the claw, whereas postlarval snapping shrimp claws – which are incapable of rapid strikes - lack this muscle (Fig. 1). One- to two-month old juvenile A. heterochaelis show a similar closer muscle orientation as adult snapping shrimp; which suggests that juveniles use a similar LaMSA mechanism as adults (Kaji et al., 2018; Ritzmann, 1974).

Elastic potential energy is stored through deformation of the propodus and possibly through stretching of the large apodeme which connects the closer muscle to the dactyl (Longo et al., In review). Exoskeletal deformation combined with stretched apodemes and other tendon-like structures are often used in other LaMSA systems for storing and releasing elastic energy. For example, locusts store some elastic energy in an apodeme when they are preparing to jump (Bennet-Clark, 1975). In snapping shrimp, the closer muscle fibers are directly inserted onto the apodeme. During contraction, the closer muscle would likely apply a strain on the apodeme, storing elastic energy. A second potential region for energy storage is the exoskeleton. Many arthropods store elastic energy in their exoskeleton, including mantis shrimp and locusts (Bennet-Clark, 1975; Zack et al., 2009). Mantis shrimp use a saddle-like structure in their exoskeleton to store and release elastic energy (Patek et al., 2007; Zack et al., 2009). Hyperbolic paraboloids, also known as saddles, are surfaces often used in engineering or architecture to distribute stresses, increasing relative stiffness, and reducing buckling or failure.

Many adult snapping shrimp species, including *Alpheus heterochaelis*, have hyperbolic paraboloids in the exoskeletons of their claws which deform and recoil during their high speed strikes (Longo et al., In review). Here we show similar bending and recoil in the saddle-like regions of juvenile claws during strikes (Movie 3). Further research is needed in order to establish how stored elastic energy is delivered to the dactyl rotation; it is likely similar to the dual spring mechanism found in trap-jaw ants (Sutton et al., 2022).

LaMSA mechanisms often vary in their presence or morphology across an organism's life history. Gall midges, bark beetles, and dragonflies use LaMSA during their larval stages but lose the mechanism when they transition to their adult morphotypes (Bertone et al., 2022; Büsse et al., 2021; Farley et al., 2019). Planthoppers nymphs use biological gears to mechanically couple their legs during high-speed jumps, but lose the gears when the nymphs molt into their adult forms (Burrows and Sutton, 2013). In snapping shrimp, the larvae do not possess a LaMSA mechanism. Even when larvae initially transition into adult habitats during settlement, they lack the snapping claws (Fig 1). It is possible that snapping shrimp must reach a certain size or age before they can develop their LaMSA mechanism; however, more research is needed to determine whether this is the case. Morphological and behavioral transitions in LaMSA offer important sources of variation that can be leveraged to explore critical morphology and biomechanical constraints on spring-actuation in biology.

Kinematic comparisons:

Juvenile *A. heterochaelis* have some of the highest recorded accelerations for repeated-use LaMSA mechanisms ($5.8 \times 10^5 \text{ m s}^{-2}$; Fig 7). Adult *A. heterochaelis* accelerations are much slower, only reaching around $2.9 \times 10^4 \text{ m s}^{-2}$ (Versluis et al., 2000). Adult snapping shrimp are over an order of magnitude greater in carapace length, around 5.5 cm total length for adults compared to 0.8 cm in juveniles (Versluis et al., 2000). Juvenile snapping shrimp angular velocities and accelerations are also an order of magnitude greater than adults (angular velocity: $27,000 \text{ rad s}^{-1}$ in juveniles vs. $3,500 \text{ rad s}^{-1}$ in adults; angular acceleration: $5.4 \times 10^8 \text{ rad s}^{-2}$ in juveniles vs. $5.8 \times 10^6 \text{ rad s}^{-2}$ in adults; Versluis et al., 2000). This would suggest that even though angular velocity did not scale significantly within the juvenile snapping shrimp sampled in this study, angular velocity would likely scale significantly when looking across the full ontogenetic size range of *A. heterochaelis*. These data support our predictions based on

mathematical models which reveal that smaller LaMSA systems generate the greatest accelerations (Ilton et al., 2018). However, while the juvenile snapping shrimp are faster than adults in terms of acceleration, the linear speed of the plunger entering the socket is greatest in adults (approximately 30 m s⁻¹ in adults and only 8 m s⁻¹ in juvenile strikes). Further research is also needed to understand how the jet of water is formed in the snapping shrimp claw across these different size scales and how closing speed affects the generation of the cavitation bubble.

Juvenile snapping shrimp strikes are similar in size and acceleration to some small trapjaw ants (Fig 7; Spagna et al., 2008). However, the juvenile strikes are particularly impressive because they must overcome the hydrodynamic drag of the water. Even with drag and added mass, snapping shrimp achieve similar accelerations as trap-jaw ants. Dracula ants and termites, which are of similar size to juvenile snapping shrimp, can achieve higher accelerations, although their strikes move through the air and not water. Jellyfish nematocysts achieve higher accelerations ($5.4 \times 10^7 \text{ m s}^{-2}$; Nüchter et al., 2006). However, smaller LaMSA mechanisms like nematocysts or fungal ballistospores can only be fired once because the mechanism fractures during energy release (Nüchter et al., 2006; Pringle et al., 2005).

Recent work in small LaMSA systems has suggested a lower size boundary for repeated-use, ultrafast motion due to a constraint on biological materials (Ilton et al., 2018; Longo et al., 2021; Sutton et al., 2019). We may be able to learn about this potential boundary by studying LaMSA development. For example, juvenile snapping shrimp develop their mechanisms near this size boundary. Why do they develop their mechanism at this size? Do other snapping shrimp and other LaMSA systems develop their mechanism at similar size scales? To our knowledge, the development of LaMSA mechanisms has been described in relatively few groups, including mantis shrimp (Harrison et al., 2021), locusts (Burrows, 2016; Gabriel, 1985), dragonfly nymphs (Büsse et al., 2021), larval gall midges (Farley et al., 2019), larval bark beetles (Bertone et al., 2022), and now snapping shrimp. Every biological LaMSA system must develop its mechanism at some point during the organism's ontogeny. These mechanisms will likely vary both morphologically and kinematically across development. Comparing relevant metrics (e.g., power density, elastic energy storage) across the life history of the organism offers an

insightful approach to exploring potential scaling and material limits in ultrafast biological motion.

Conclusion:

This study establishes the development and kinematics of the big-claw snapping shrimp (*Alpheus heterochaelis*) snapping claw and LaMSA mechanism. Juvenile *A. heterochaelis* strikes are the highest reported accelerations for underwater, repeated-use LaMSA movements. The snapping claw develops between one- to two months after snapping shrimp settle as postlarvae. Even at the millimeter size, juvenile snapping shrimp strikes generate cavitation bubbles that produce audible sounds. The juvenile snapping shrimp LaMSA mechanism appears to use a similar torque-reversal latch seen in their adult counterparts. These findings offer insights into the development of LaMSA systems and potential limits to repeated-use and ultrafast motion. They also encourage engineering innovations of LaMSA at far smaller size scales than are reflected in current innovations of physical models and robotic systems (Armour et al., 2007; Büsse et al., 2021; Divi et al., 2020; Hawkes et al., 2022; Hess et al., 2013; Kim et al., 2021; Koukouvinis et al., 2017; Steinhardt et al., 2021).

Acknowledgements

- Special thanks to J. Dinh for help collecting specimens. Thanks to S. Longo, J. Jorge, W. Ray, S.
- 566 Cox, and B. Schelling for their advice and feedback during the project. Thank you to the
- Impulsive MURI team for feedback. Special thanks to G. Budziszewski for her support.

Competing Interests

570 The authors declare no competing or financial interests.

Author contributions

- 573 Conceptualization: J.S.H, S.N.P.; Methodology: J.S.H, S.N.P.; Formal Analysis: J.S.H.;
- Investigation: J.S.H.; Resources: J.S.H., S.N.P.; Data curation: J.S.H.; Writing original draft:
- J.S.H., S.N.P.; Writing review & editing: J.S.H., S.N.P.; Visualization: J.S.H.; Supervision: S.N.P.;
- 576 Project Administration: S.N.P.; Funding acquisition: S.N.P.

578	Funding
579	This material is based upon work supported by, or in part by, the US Army Research Laboratory
580	and the US Army Research Office under contract/grant W911NF1510358 and the National
581	Science Foundation (NSF IOS 2019323).
582	
583	
584	Data availability
585	All datasets and computer coding are available from the Dryad Digital Repository (Harrison and
586	Patek, 2022): Dryad numbers provided upon acceptance.

Figure Legends

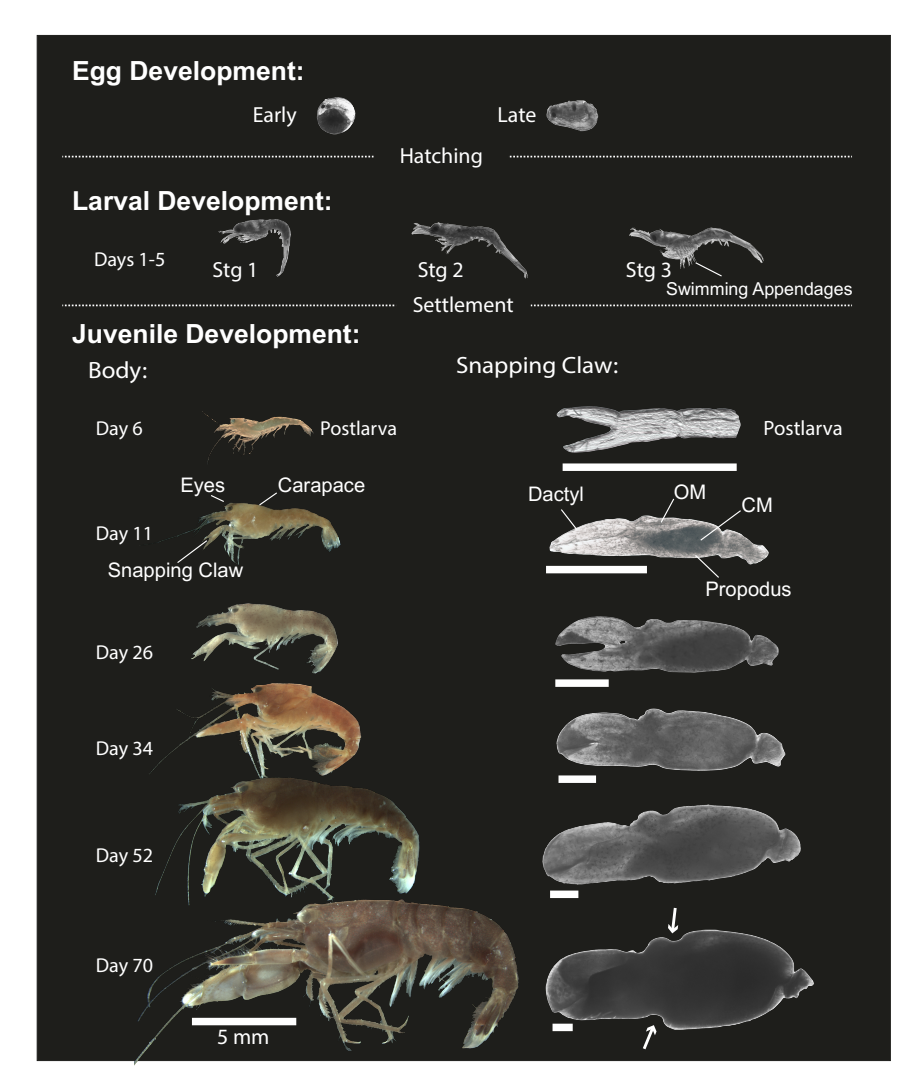


Figure 1: Juvenile snapping shrimp develop their LaMSA morphology between one- and two-months post-settlement.

Developmental sequence of *Alpheus heterochaelis* and their snapping claws through the first seventy days post-hatching. At the postlarval stage, the first pereopods are undifferentiated chelae which differentiate after several molts. Snapping claws on the right correspond with the individuals shown to their left. The images of the snapping shrimp are scaled relative to the 5-millimeter scale bar shown below the bottom snapping shrimp. The arrows on the bottom snapping claw indicate the saddle-like regions developing on the propodus exoskeleton. Solid horizontal scale bars beneath snapping claws represent one millimeter.

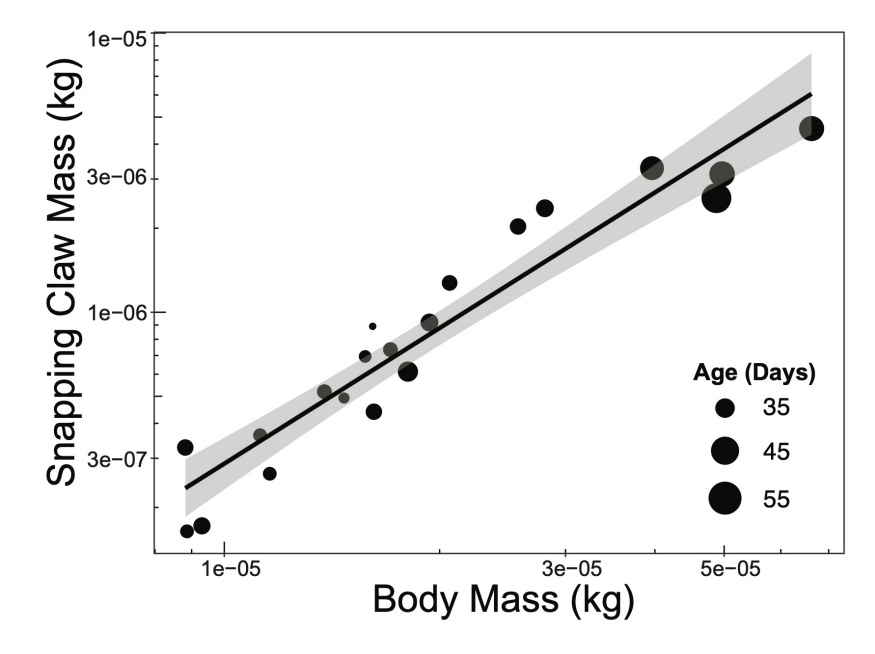


Figure 2: Larger snapping shrimp have larger snapping claws and are generally older. Scaling of claw mass relative to body mass in an ontogenetic series of snapping shrimp. Points represent several snapping shrimp individuals (n=20) at different ages. Size of points represent age.

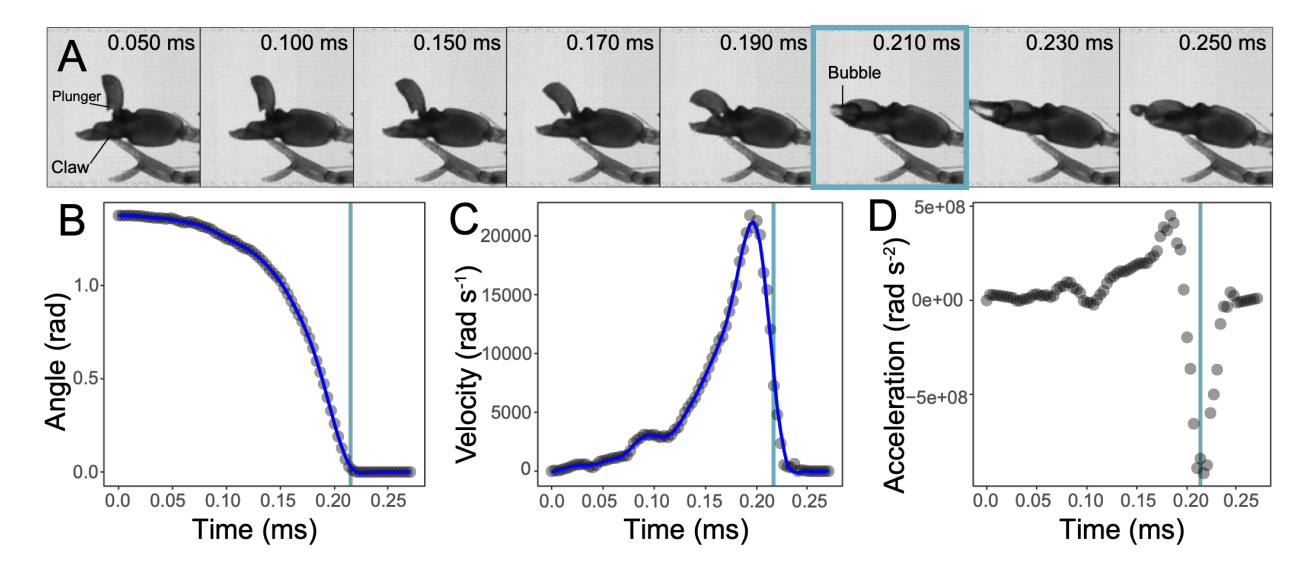


Figure 3: Juvenile snapping shrimp rapidly close their snapping claws and produce cavitation bubbles.

(A) A subset of a high speed image sequence of a juvenile snapping shrimp strike shows the

dactyl swinging shut and generating a cavitation bubble that is ejected away from the claw (to

the left of the page). The kinematics of the snapping shrimp strike shown in panel A in terms of the dactyl's angle (B), angular velocity (C), and angular acceleration (D). Blue lines represent LOESS models fit to the data and used to calculate the derivative with respect to time. High speed video was filmed at 300,000 frames per second. Vertical blue line in kinematic panels represents the frame highlighted in panel A. The juvenile snapping shrimp featured here was 37 days old with a 2 mg snapping claw.

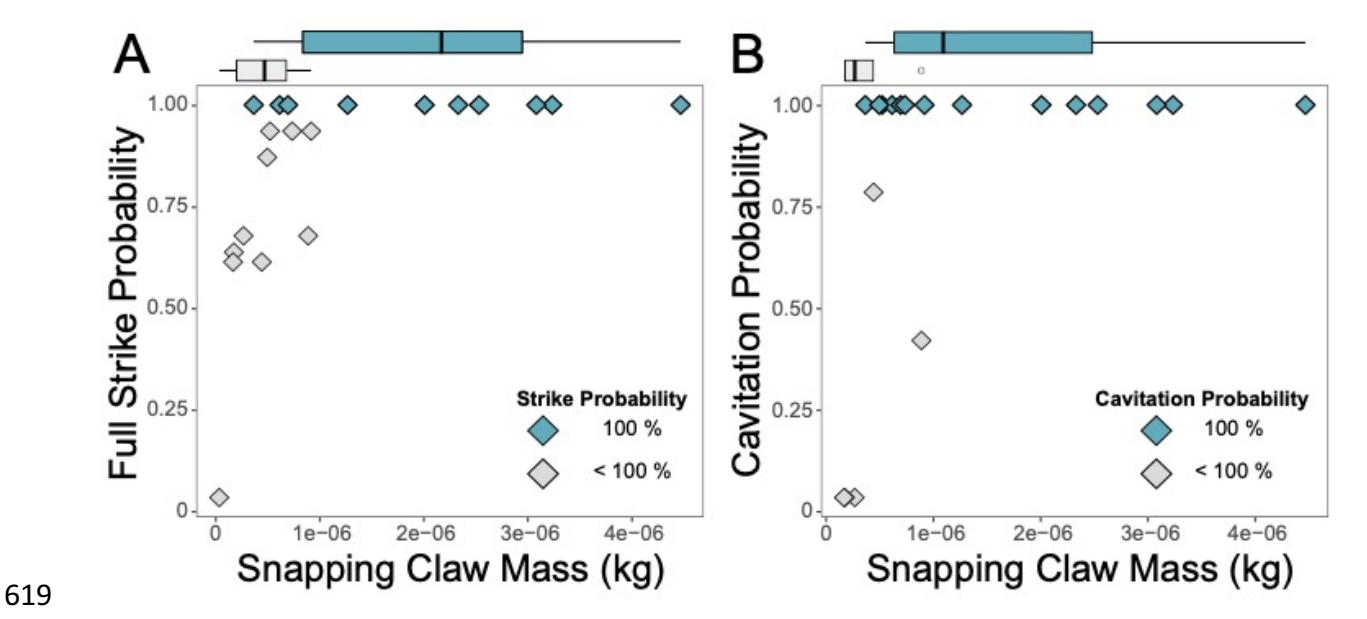


Figure 4: Juvenile snapping shrimp with larger claws strike and produce cavitation bubbles more reliably than shrimp with smaller claws.

(A) The probability that individual snapping shrimp produce full strikes. Full strikes are defined as snaps during which the dactyl completely closes against the propodus. (B) The probability that an individual snapping shrimp produces cavitation bubbles during full strikes. Green points represent individuals that generated full strikes or cavitation bubbles 100% of the time. Grey points represent individuals that sometimes did not complete a strike or did not cavitate. The boxplots represent the spread of individuals shown in the corresponding panel below. The line in the box represents the median, the box encompasses the middle 50% of the data, and the whiskers represent the bottom and top 25% of data values. Points on the box plots represent outliers.

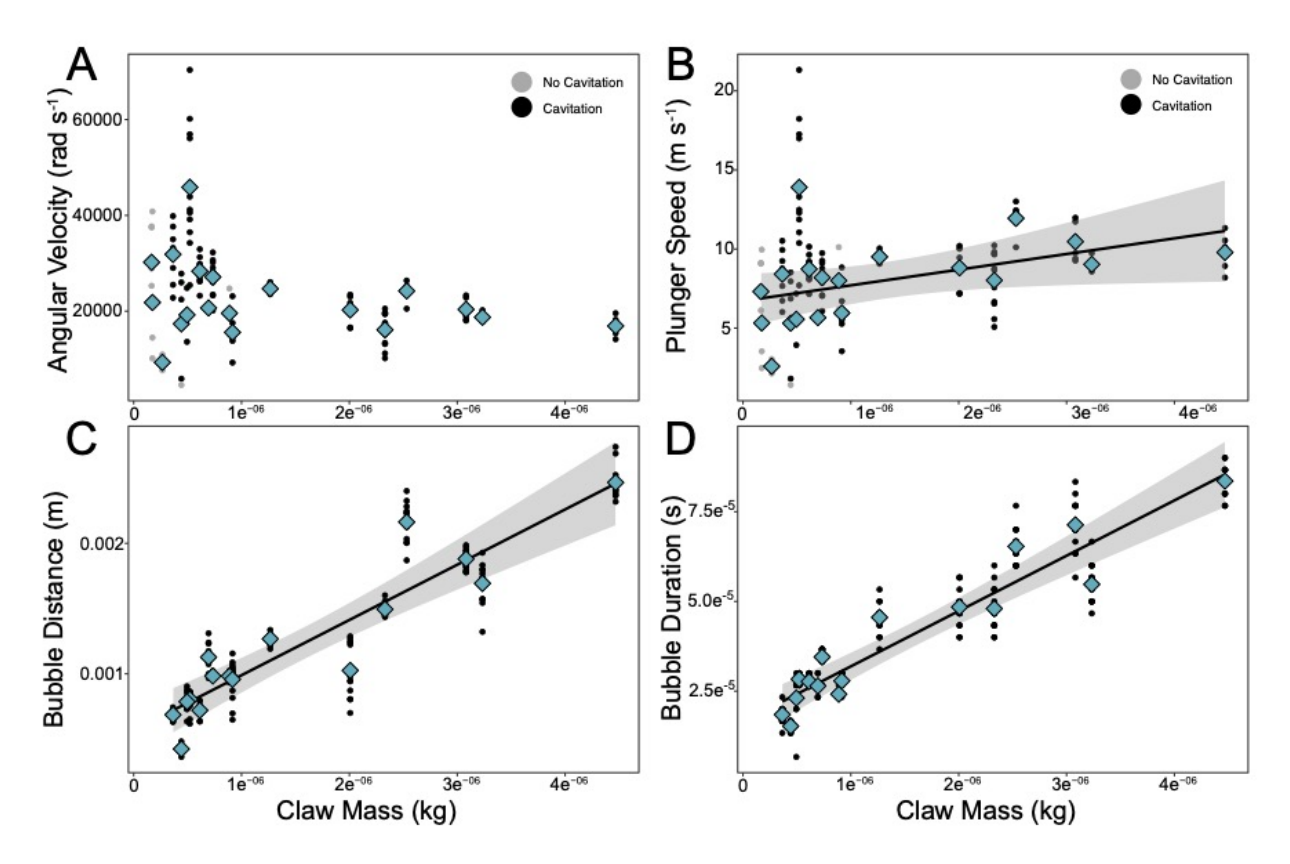


Figure 5: Larger snapping claws do not rotate faster than smaller claws, although the plunger enters the socket at a higher speed in larger claws. Larger snapping claws generate bubbles that last longer and travel further than smaller snapping claws.

Scaling of snapping shrimp claw mass relative to claw kinematics and bubble dynamics during high speed strikes. Claw kinematics include the peak angular velocity of the strike (A) and the peak linear speed of the plunger during a strike (B). Bubble dynamics include the maximum distance traveled (C) and the total collapse duration (D) of the cavitation bubble. Blue diamonds represent individual averages and circles represent individual strikes. Black points represent strikes that produced cavitation, gray points are strikes that did not cavitate. Lines represent significant linear regressions using individual averages and the shaded regions represent their 95% CI.

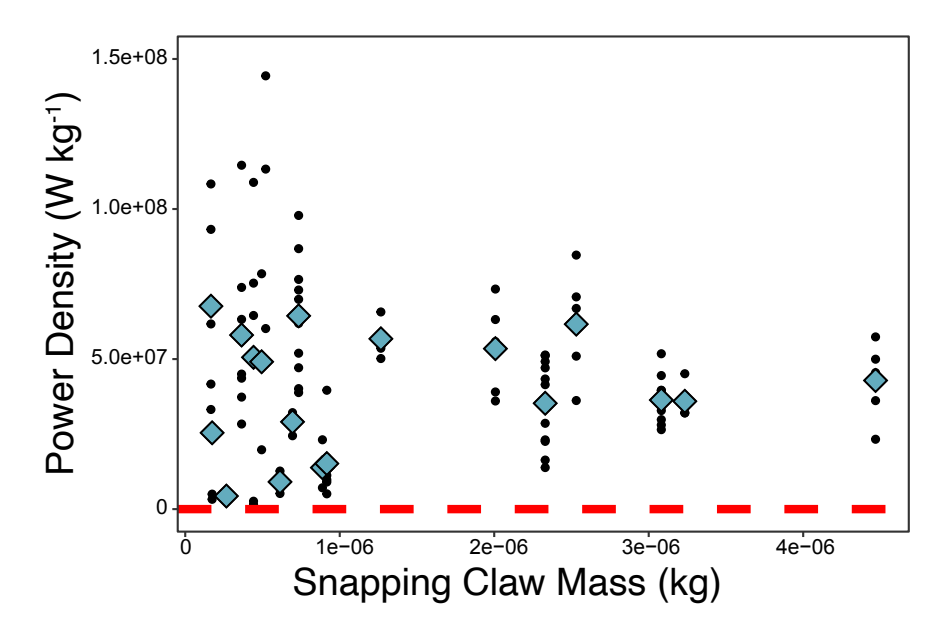
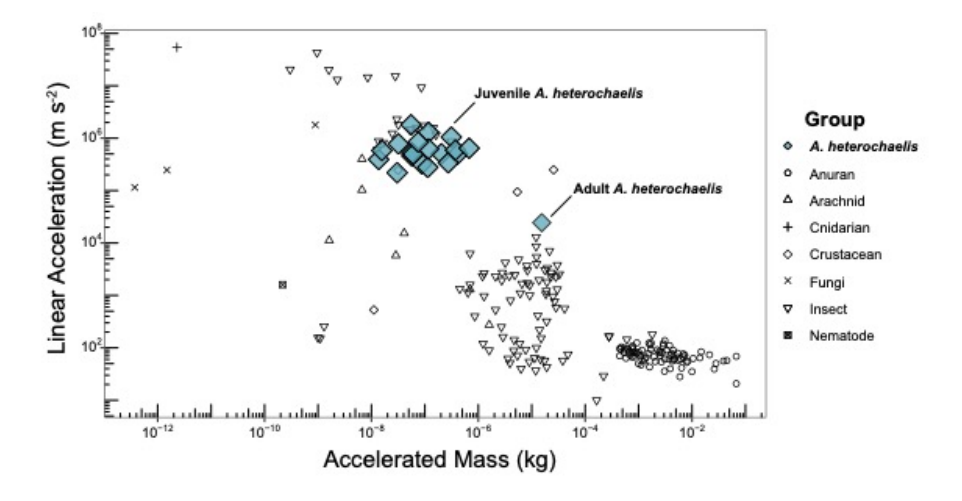


Figure 6: Power density of juvenile snapping shrimp strikes show that their ultrafast movements are powered by spring actuation.

(A) The power density of juvenile snapping shrimp strikes exceeds muscle power limits.

Therefore, juvenile snapping shrimp must use stored elastic energy to generate their high speed snaps. The red dashed line represents the maximum power output of vertebrate muscle, 1200 W kg⁻¹ (Askew et al., 2001). Blue diamonds are individual averages. Black circles represent power density of strikes.



654 Figure 7: Juvenile snapping shrimp strikes achieve accelerations over an order of magnitude 655 greater than adults. 656 Linear acceleration of high-acceleration systems compared to the mass of the accelerated 657 object. Shapes of the points represent taxonomic grouping (n=198 species), green diamonds 658 represent snapping shrimp. Data includes both repeated and non-repeated use LaMSA 659 mechanisms. Original comparative dataset was compiled from Ilton et al., 2018 and Patek, 660 2019; we further added 106 additional species from published literature. References are 661 available in Supplementary Table 2.

Table 1: Average strike kinematics of juvenile A. heterochaelis.

4 5

Individuals	Strikes per individual	Carapace Length (m x 10 ⁻³)	Claw Mass (kg x 10 ⁻⁷)	Dactyl Mass (kg x 10 ⁻⁸)	Strike Duration (s x 10 ⁻⁴)	Angular Displacement (rad)	Angular Velocity (rad s ⁻¹ x 10 ⁴)	Angular Acceleration (rad s ⁻² x 10 ⁸)	Plunger Speed (m s ⁻¹)	Linear Acceleration (m s ⁻² x 10 ⁵)	Strike Energy (J x 10 ⁻	Power Density (W kg ⁻¹ x 10 ⁷)
19	6	4.1	13.259	16.21	3.2730	1.34	2.26	5.4	8.0	5.8	1.7	4.3
	(2 – 13)	(3.1-5.9)	(1.663-	(1.37-	(2.0330-	(0.86-2.14)	(1.56-9.30)	(1.5-16.5)	(2.6-	(1.4-15.1)	(0.04*-	(0.4-
			44.683)	67.23)	6.1166)				13.9)		7.3)	18.0)

Numbers represent the mean with the minimum and maximum values in parentheses. Numbers marked with asterisk (*) are less than the uncertainty of the measurement.

1	References:
2	Alexander, S. L. M. and Bhamla, M. S. (2020). Ultrafast launch of slingshot spiders using conical silk webs. <i>Curr. Biol.</i> 30 , R928–R929.
4 5	Anderson, P. S. L., Claverie, T. and Patek, S. N. (2014). Levers and linkages: Mechanical tradeoffs in a power-amplified system. <i>Evolution</i> 68 , 1919–1933.
6 7 8	Anker, A., Ahyong, S. T., Noel, P. Y. and Palmer, A. R. (2006). Morphological phylogeny of Alpheid shrimps: Parallel preadaptation and the origin of a key morphological innovation, the snapping claw. <i>Evolution</i> 60 , 2507–2528.
9 10	Armour, R., Paskins, K., Bowyer, A., Vincent, J. and Megill, W. (2007). Jumping robots: a biomimetic solution to locomotion across rough terrain. <i>Bioinspir. Biomim.</i> 2 , S65.
11 12 13	Askew, G. N., Marsh, R. L. and Ellington, C. P. (2001). The mechanical power output of the flight muscles of blue-breasted quail (<i>Coturnix chinensis</i>) during take-off. <i>J. Exp. Biol.</i> 204 , 3601–3619.
14 15	Bennet-Clark, H. C. (1975). The energetics of the jump of the locust <i>Schistocerca gregaria</i> . <i>J. Exp. Biol.</i> 63 , 53–83.
16 17 18	Bertone, M. A., Gibson, J. C., Seago, A. E., Yoshida, T. and Smith, A. A. (2022). A novel power-amplified jumping behavior in larval beetles (Coleoptera: Laemophloeidae). <i>PLOS ONE</i> 17 , e0256509.
19 20	Blanco, M. M. and Patek, S. N. (2014). Muscle trade-offs in a power-amplified prey capture system. <i>Evolution</i> 68 , 1399–1414.
21 22 23 24	Booher, D. B., Gibson, J. C., Liu, C., Longino, J. T., Fisher, B. L., Janda, M., Narula, N., Toulkeridou, E., Mikheyev, A. S., Suarez, A. V., et al. (2021). Functional innovation promotes diversification of form in the evolution of an ultrafast trap-jaw mechanism in ants. <i>PLOS Biol.</i> 19 , e3001031.
25 26 27	Brunt, L. H., Begg, K., Kague, E., Cross, S. and Hammond, C. L. (2017). Wnt signalling controls the response to mechanical loading during zebrafish joint development. <i>Development</i> 144 , 2798–2809.
28 29	Burrows, M. (2016). Development and deposition of resilin in energy stores for locust jumping. <i>J. Exp. Biol.</i> 219 , 2449–2457.
30 31	Burrows, M. and Sutton, G. (2013). Interacting gears synchronize propulsive leg movements in a jumping insect. <i>Science</i> 341 , 1254–1256.

32	Büsse, S., Koehnsen, A., Rajabi, H. and Gorb, S. N. (2021). A controllable dual-catapult system
33	inspired by the biomechanics of the dragonfly larvae's predatory strike. Sci. Robot. 6,
34	eabc8170.
35	Butler, J., Butler, M. J. and Gaff, H. (2017). Snap, crackle, and pop: Acoustic-based model
36	estimation of snapping shrimp populations in healthy and degraded hard-bottom
37	habitats. <i>Ecol. Indic.</i> 77 , 377–385.
38	Chow, L. H., De Grave, S., Anker, A., Poon, K. K. Y., Ma, K. Y., Chu, K. H., Chan, TY. and Tsang,
39	L. M. (2021). Distinct suites of pre- and post-adaptations indicate independent
40	evolutionary pathways of snapping claws in the shrimp family Alpheidae (Decapoda:
41	Caridea). <i>Evolution</i> 75 , 2898–2910.
42	Claverie, T. and Patek, S. N. (2013). Modularity and rates of evolutionary change in a power-
43	amplified prey capture system. Evolution 67, 3191–3207.
44	Dangles, O., Pierre, D., Christides, J. P. and Casas, J. (2007). Escape performance decreases
45	during ontogeny in wild crickets. J. Exp. Biol. 210, 3165–3170.
46	Dinh, J. P. and Patek, S. N. Weapon performance and contest assessment strategies of the
47	cavitating snaps in snapping shrimp. Funct. Ecol. n/a,.
48	Dinh, J. P., Azza, J. and Patek, S. N. (2020). Winner effects and switching assessment strategies
49	facilitate fast and frugal decisions in territorial contests. <i>Anim. Behav.</i> 170 , 189–205.
50	Divi, S., Ma, X., Ilton, M., St. Pierre, R., Eslami, B., Patek, S. N. and Bergbreiter, S. (2020).
51	Latch-based control of energy output in spring actuated systems. J. R. Soc. Interface 17,
52	20200070.
53	Farley, G. M., Wise, M. J., Harrison, J. S., Sutton, G. P., Kuo, C. and Patek, S. N. (2019).
54	Adhesive latching and legless leaping in small, worm-like insect larvae. J. Exp. Biol. 222,
55	jeb201129.
56	Fernandes, J. J., Celniker, S. E. and VijayRaghavan, K. (1996). Development of the indirect flight
57	muscle attachment sites in Drosophila: Role of the PS integrins and the stripe gene. Dev.
58	<i>Biol.</i> 176 , 166–184.
59	Freckleton, R. P. and Jetz, W. (2009). Space versus phylogeny: disentangling phylogenetic and
60	spatial signals in comparative data. <i>Proc. R. Soc. B Biol. Sci.</i> 276 , 21–30.
61	Gabriel, J. M. (1985). The development of the locust jumping mechanism: I. Allometric growth
62	and its effect on jumping performance. J. Exp. Biol. 118, 313–326.

Gibson, J. C., Larabee, F. J., Touchard, A., Orivel, J. and Suarez, A. V. (2018). Mandible strike

kinematics of the trap-jaw ant genus Anochetus Mayr (Hymenoptera: Formicidae). J.

63

64

65

Zool. **306**, 119–128.

- Govind, C. K., Wong, A. and Pearce, J. (1988). Experimental induction of claw transformation in
 snapping shrimps. J. Exp. Zool. 248, 371–375.
- Gronenberg, W. (1996). Fast actions in small animals: springs and click mechanisms. *J. Comp. Physiol. A* 178, 727–734.
- Harrison, J. S., Porter, M. L., McHenry, M. J., Robinson, H. E. and Patek, S. N. (2021). Scaling
 and development of elastic mechanisms: the tiny strikes of larval mantis shrimp. *J. Exp. Biol.* 224, jeb235465.
- Hawkes, E. W., Xiao, C., Peloquin, R.-A., Keeley, C., Begley, M. R., Pope, M. T. and Niemeyer,
 G. (2022). Engineered jumpers overcome biological limits via work multiplication.
 Nature 604, 657–661.
- Hedrick, T. L. (2008). Software techniques for two- and three-dimensional kinematic
 measurements of biological and biomimetic systems. *Bioinspir. Biomim.* 3, 034001.
- Hernandez, L. P. (2000). Intraspecific scaling of feeding mechanics in an ontogenetic series of zebrafish, *Danio rerio. J. Exp. Biol.* **203**, 3033–3043.
- Herrel, A. and Gibb, A. C. (2006). Ontogeny of performance in vertebrates. *Physiol. Biochem.* Zool. 79, 1–6.
- Hess, D., Brücker, C., Hegner, F., Balmert, A. and Bleckmann, H. (2013). Vortex formation with a snapping shrimp claw. *PLOS ONE* **8**, e77120.
- Hoerner, S. F. (1965). Fluid-dynamic drag. Theoretical, experimental, and statistical information. *Copyr. SF Hoerner Fluid Dyn. Vanc. Print. USA Card Number 64-19666*.
- Hofhuis, H., Moulton, D., Lessinnes, T., Routier-Kierzkowska, A.-L., Bomphrey, R. J., Mosca, G.,
 Reinhardt, H., Sarchet, P., Gan, X., Tsiantis, M., et al. (2016). Morphomechanical innovation drives explosive seed dispersal. *Cell* 166, 222–233.
- Hughes, M. (1996). Size assessment via a visual signal in snapping shrimp. *Behav. Ecol.* Sociobiol. 38, 51–57.
- 91 Ilton, M., Bhamla, M. S., Ma, X., Cox, S. M., Fitchett, L. L., Kim, Y., Koh, J., Krishnamurthy, D., 92 Kuo, C.-Y., Temel, F. Z., et al. (2018). The principles of cascading power limits in small, 93 fast biological and engineered systems. *Science* **360**, eaao1082.
- 94 **Ilton, M., M. Cox, S., Egelmeers, T., P. Sutton, G., N. Patek, S. and J. Crosby, A.** (2019). The 95 effect of size-scale on the kinematics of elastic energy release. *Soft Matter* **15**, 9579– 96 9586.
- 97 **Kaji, T., Anker, A., Wirkner, C. S. and Palmer, A. R.** (2018). Parallel saltational evolution of ultrafast movements in snapping shrimp claws. *Curr. Biol.* **28**, 106-113.e4.

- Kim, B.-N., Hahn, J., Choi, B. K. and Kim, B.-C. (2010). Snapping shrimp sound measured under
 laboratory conditions. *Jpn. J. Appl. Phys.* 49, 07HG04.
- 101 **Kim, Y., van den Berg, J. and Crosby, A. J.** (2021). Autonomous snapping and jumping polymer 102 gels. *Nat. Mater.* **20**, 1695–1701.
- Kingston, A. C. N., Woodin, S. A., Wethey, D. S. and Speiser, D. I. (2022). Snapping shrimp have helmets that protect their brains by dampening shock waves. *Curr. Biol.* **32**, 3576-3583.e3.
- 106 **Knowlton, R. E.** (1973). Larval development of the snapping shrimp *Alpheus heterochaelis* Say, 107 reared in the laboratory. *J. Nat. Hist.* **7**, 273–306.
- Kolmann, M. A. and Huber, D. R. (2009). Scaling of feeding biomechanics in the horn shark
 Heterodontus francisci: ontogenetic constraints on durophagy. *Zoology* 112, 351–361.
- 110 **Koukouvinis, P., Bruecker, C. and Gavaises, M.** (2017). Unveiling the physical mechanism behind pistol shrimp cavitation. *Sci. Rep.* **7**, 13994.
- Larabee, F. J., Gronenberg, W. and Suarez, A. V. (2017). Performance, morphology and control of power-amplified mandibles in the trap-jaw ant *Myrmoteras* (Hymenoptera: Formicidae). *J. Exp. Biol.* **220**, 3062–3071.
- Larabee, F. J., Smith, A. A. and Suarez, A. V. (2018). Snap-jaw morphology is specialized for
 high-speed power amplification in the Dracula ant, Mystrium camillae. *R. Soc. Open Sci.* 5, 181447.
- Lohse, D., Schmitz, B. and Versluis, M. (2001). Snapping shrimp make flashing bubbles. *Nature*413, 477–478.
- Longo, S. J., Cox, S. M., Azizi, E., Ilton, M., Olberding, J. P., St Pierre, R. and Patek, S. N. (2019).
 Beyond power amplification: latch-mediated spring actuation is an emerging framework
 for the study of diverse elastic systems. *J. Exp. Biol.* 222, jeb197889.
- Longo, S. J., Ray, W., Farley, G. M., Harrison, J., Jorge, J., Kaji, T., Palmer, A. R. and Patek, S. N.
 (2021). Snaps of a tiny amphipod push the boundary of ultrafast, repeatable movement.
 Curr. Biol. 31, R116–R117.
- Longo, S. J., St Pierre, R., Bergbreiter, S., Schelling, B. and Patek, S. N. (In review). Geometric
 latches can reduce or enhance variable outputs of ultrafast, spring-propelled systems.
- Mathews, L. M., Schubart, C. D., Neigel, J. E. and Felder, D. L. (2002). Genetic, ecological, and behavioural divergence between two sibling snapping shrimp species (Crustacea: Decapoda: Alpheus). *Mol. Ecol.* **11**, 1427–1437.

131 McHenry, M. J., Claverie, T., Rosario, M. V. and Patek, S. N. (2012). Gearing for speed slows 132 the predatory strike of a mantis shrimp. J. Exp. Biol. 215, 1231–1245. 133 McHenry, M. J., Anderson, P. S. L., Van Wassenbergh, S., Matthews, D. G., Summers, A. P. and 134 Patek, S. N. (2016). The comparative hydrodynamics of rapid rotation by predatory 135 appendages. J. Exp. Biol. 219, 3399-3411. 136 Mendoza, E., Azizi, E. and Moen, D. S. (2020). What explains vast differences in jumping power 137 within a clade? Diversity, ecology and evolution of anuran jumping power. Funct. Ecol. 138 **34**, 1053–1063. 139 Moen, D. S., Irschick, D. J. and Wiens, J. J. (2013). Evolutionary conservatism and convergence 140 both lead to striking similarity in ecology, morphology and performance across 141 continents in frogs. Proc. R. Soc. B Biol. Sci. 280, 20132156. 142 Moen, D. S., Ravelojaona, R. N., Hutter, C. R. and Wiens, J. J. (2021). Testing for adaptive 143 radiation: A new approach applied to Madagascar frogs. Evolution 75, 3008-3025. 144 Muñoz, M. M. (2022). The Bogert effect, a factor in evolution. *Evolution* 76, 49–66. 145 Nolan, B. and Salmon, M. (1970). The behavior and ecology of snapping shrimp (Crustacea: 146 Alpheus heterochelis and Alpheus normanni). 2, 289–335. 147 Nowlan, N. C., Sharpe, J., Roddy, K. A., Prendergast, P. J. and Murphy, P. (2010). 148 Mechanobiology of embryonic skeletal development: Insights from animal models. Birth 149 Defects Res. Part C Embryo Today Rev. **90**, 203–213. 150 Nüchter, T., Benoit, M., Engel, U., Özbek, S. and Holstein, T. W. (2006). Nanosecond-scale kinetics of nematocyst discharge. Curr. Biol. 16, R316–R318. 151 152 Patek, S. N. (2019). The power of mantis shrimp strikes: interdisciplinary impacts of an extreme 153 cascade of energy release. Integr. Comp. Biol. 59, 1573–1585. 154 Patek, S. N., Korff, W. L. and Caldwell, R. L. (2004). Deadly strike mechanism of a mantis 155 shrimp. *Nature* **428**, 819–820. 156 Patek, S. N., Nowroozi, B. N., Baio, J. E., Caldwell, R. L. and Summers, A. P. (2007). Linkage 157 mechanics and power amplification of the mantis shrimp's strike. J. Exp. Biol. 210, 3677— 158 3688. 159 Patek, S. N., Dudek, D. M. and Rosario, M. V. (2011). From bouncy legs to poisoned arrows: 160 elastic movements in invertebrates. J. Exp. Biol. 214, 1973–1980.

Pringle, A., Patek, S. N., Fischer, M., Stolze, J. and Money, N. P. (2005). The captured launch of

a ballistospore. Mycologia 97, 866–871.

161

162

163 Ritzmann, R. E. (1974). Mechanisms for the snapping behavior of two alpheid shrimp, Alpheus 164 californiensis and Alpheus heterochelis. J. Comp. Physiol. 95, 217–236. 165 Roberts, T. J. and Azizi, E. (2011). Flexible mechanisms: the diverse roles of biological springs in 166 vertebrate movement. J. Exp. Biol. 214, 353–361. 167 Rosario, M. V. and Patek, S. N. (2015). Multilevel analysis of elastic morphology: The mantis 168 shrimp's spring. J. Morphol. 276, 1123–1135. 169 Sarpkaya, T. (1986). Force on a circular cylinder in viscous oscillatory flow at low Keulegan— 170 Carpenter numbers. J. Fluid Mech. 165, 61–71. 171 Schein, H. (1977). The role of snapping in Alpheus heterochaelis Say, 1818, the Big-Clawed 172 Snapping Shrimp. *Crustaceana* **33**, 182–188. 173 Schneider, C. A., Rasband, W. S. and Eliceiri, K. W. (2012). NIH Image to ImageJ: 25 years of 174 image analysis. Nat. Methods 9, 671–675. 175 Seid, M. A., Scheffrahn, R. H. and Niven, J. E. (2008). The rapid mandible strike of a termite 176 soldier. Curr. Biol. 18, R1049-R1050. 177 Spagna, J. C., Vakis, A. I., Schmidt, C. A., Patek, S. N., Zhang, X., Tsutsui, N. D. and Suarez, A. V. 178 (2008). Phylogeny, scaling, and the generation of extreme forces in trap-jaw ants. J. Exp. 179 Biol. 211, 2358-2368. 180 Spence, H. R. and Knowlton, R. E. (2008). Morphological and developmental differences in 181 three species of the snapping shrimp genus Alpheus (Crustacea, Decapoda). Southeast. 182 *Nat.* **7**, 207–218. 183 Steinhardt, E., Hyun, N. P., Koh, J., Freeburn, G., Rosen, M. H., Temel, F. Z., Patek, S. N. and 184 Wood, R. J. (2021). A physical model of mantis shrimp for exploring the dynamics of 185 ultrafast systems. Proc. Natl. Acad. Sci. 118, e2026833118. 186 Sutton, G. P., Mendoza, E., Azizi, E., Longo, S. J., Olberding, J. P., Ilton, M. and Patek, S. N. (2019). Why do large animals never actuate their jumps with latch-mediated springs? 187 188 Because they can jump higher without them. *Integr. Comp. Biol.* **59**, 1609–1618. 189 Sutton, G. P., St Pierre, R., Kuo, C.-Y., Summers, A. P., Bergbreiter, S., Cox, S. and Patek, S. N. 190 (2022). Dual spring force couples yield multifunctionality and ultrafast, precision 191 rotation in tiny biomechanical systems. J. Exp. Biol. 225,.

Tang, X. and Staack, D. (2019). Bioinspired mechanical device generates plasma in water via

cavitation. Sci. Adv. 5, eaau7765.

192

193

194 195 196	Tanner, J. B., Zelditch, M. L., Lundrigan, B. L. and Holekamp, K. E. (2010). Ontogenetic change in skull morphology and mechanical advantage in the spotted hyena (Crocuta crocuta). <i>J. Morphol.</i> 271 , 353–365.
197 198	Versluis, M., Schmitz, B., von der Heydt, A. and Lohse, D. (2000). How snapping shrimp snap: through cavitating bubbles. <i>Science</i> 289 , 2114–2117.
199 200 201	Vincent, S. E., Moon, B. R., Herrel, A. and Kley, N. J. (2007). Are ontogenetic shifts in diet linked to shifts in feeding mechanics? Scaling of the feeding apparatus in the banded watersnake Nerodia fasciata. <i>J. Exp. Biol.</i> 210, 2057–2069.
202 203	Warton, D. I., Duursma, R. A., Falster, D. S. and Taskinen, S. (2012). smatr 3– an R package for estimation and inference about allometric lines. <i>Methods Ecol. Evol.</i> 3, 257–259.
204 205	Wood, H. M. (2020). Morphology and performance of the 'trap-jaw' cheliceral strikes in spiders (Araneae, Mecysmaucheniidae). <i>J. Exp. Biol.</i> 223 , jeb219899.
206 207 208	Yang, Y., Qin, S., Di, C., Qin, J., Wu, D. and Zhao, J. (2020). Research on claw motion characteristics and cavitation bubbles of snapping shrimp. <i>Appl. Bionics Biomech.</i> 2020 , e6585729.
209 210	Young, R. E., Pearce, J. and Govind, C. K. (1994). Establishment and maintenance of claw bilateral asymmetry in snapping shrimps. <i>J. Exp. Zool.</i> 269 , 319–326.
211 212	Zack, T. I., Claverie, T. and Patek, S. N. (2009). Elastic energy storage in the mantis shrimp's fast predatory strike. <i>J. Exp. Biol.</i> 212, 4002–4009.
213	
214	